ESCOLA SUPERIOR DE TECNOLOGIA DA SAÚDE DE LISBOA
INSTITUTO POLITÉCNICO DE LISBOA

Lisbon School of Health Technology

Master in Radiations Applied to Health Technologies

Evaluation of the truncation artifact in cardiac PET-CT images acquired with Rb-82

Dissertation for obtaining the Degree of Master

Author: Raquel Gaspar

Supervisors: Dr Luís Freire
Dr Ian Armstrong

Lisbon, July 2020

Acknowledgements

First, I would like to give a big thank you to my supervisors, Dr Luís Freire for all his support and feedback throughout the development of this thesis; to Dr Ian Armstrong for all his support, guidance and feedback which were essential for the development of this thesis. I would also like to thank to the Nuclear Medicine Department of the Manchester Royal Infirmary for giving me the opportunity to develop this project.

I would also like to thank my family, especially my father for all his support throughout this journey.

A big thank you to my friends for all the support, specially to Maria Clara Alves who helped me with the idea for the project and for her support which without it this thesis would not be possible.

Abstract

Introduction: In all available PET-CT systems, standard FOV of the CT scanner is 50 cm, which is slightly smaller than the one of PET scanner. This difference between the two scanners may lead to truncation artifacts, causing some sections of the PET emission data not to have any corresponding attenuation-correction map. This investigation aims to evaluate the influence of TOF-based reconstruction on the truncation artifact when performing cardiac PET-CT exams with Rb-82 and, additionally, to evaluate the influence of this artifact in clinical images.

Method: 73 resting studies of myocardial perfusion with Rb-82 – obtained at the Nuclear Medicine Department of the Manchester Royal Infirmary – were selected. CT reconstructions were performed with the standard 50 cm FOV and the 78 cm extended FOV. Truncation on the 50 cm FOV was identified on a pure visual basis and performed by applying a wide image window to the CT, which showed the extent of the reconstructed FOV. TOF and Non-TOF PET images were reconstructed with both the 50cm CT and extended FOV CT. A ratio image was produced by dividing the voxel values of the PET using the 50cm CT by the voxel values of the PET using the extended CT image on a voxel by-voxel basis. A visual quality assessment was also performed to verify differences between truncated and non-truncated images, with and without TOF.

Results: When comparing voxel ratios for non-TOF and TOF reconstructions, a significantly greater variation in the truncated images compared with the non-truncated images was observed. It was also verified that when compared between male and female there was no significant differences on the impact of the truncation artifact.

Conclusion: Truncation artifact is more prevalent in patients with large body mass index. Besides, TOF reconstruction may be more robust, and reduce the impact of the CT truncation and therefore is the method of choice for patients with large body mass index.

Keywords: PET-CT, Rb-82, Truncation, TOF.

Contents

List of figures

List of tables

List of acronyms

A	
AC	Attenuation Coefficient
C	
CAD	Coronary Artery Disease
CT	Computed tomography
F	
F-18	Fluorine-18
FOV	Field of view
H	
HU	Hounsfield Units
L	
LOR	Line of response
LVEF	Left Ventricular Ejection Fraction
P	
PET	Positron emission tomography
R	
Rb-82	Rubidium-82
S	
SiPM	Silicon photomultiplier
Sr-82	Strontium-82
SNR	Signal-to-noise Ratio
T	
TOF	Time-of-flight

1 Introduction

With the recent advances in technology and medical imaging, Positron Emission Tomography (PET) has been considered to be one of the most sensitive in-vivo and less/non-invasive molecular imaging modality[7][13].

In the beginning of the 80's, medical imaging gained a greater interest due to the commercial production of PET systems. In the 60's, the first cyclotron was produced at the Hammersmith Hospital (London, UK) and Washington University[2]. Since then, the use of gamma radiation emitting sources in the medical field has seen an increase around the world. In the last decade, there have been considerable advances in the instrumentation of the camera aiming the improvement of the diagnostic techniques and the reduction of image artifacts[2].

1.1 Aim of this Thesis

In all available Positron Emission Tomography - Computed Tomography (PET-CT) systems, standard field of view (FOV) of the Computed tomography (CT) scanner is 50 cm, which is slightly smaller than the one of the PET scanners. This difference between the two scanners may lead to truncation artifacts, caused by the fact that some sections of the PET emission data not to have any corresponding attenuation-correction map. This investigation aims to evaluate the truncation artifact when performing cardiac PET-CT exams with rubidium-82 (Rb-82). This evaluation will be done considering several parameters, namely the prevalence, the influence of using Time-of-flight (TOF) reconstruction technology on images with the artifact and the influence of these on the clinical aspect of the images. The conduction of this research on Rb-82 PET-CT scans rather than on FDG PET-CT ones is due to the substantial number of the former performed in the department and to the far less literature regarding the truncation artifact in this type of scans.

1.2 Organization of this Thesis

This thesis is organized into 6 chapters. In Chapter 2, the fundamentals of PET (and PET-CT) systems, TOF reconstruction and cardiac PET-CT with rubidium-82 are presented. Chapter 3 presents the method used to conduct this work and, in Chapter 4, the results and are presented. Finally, in Chapters 5 and 6, the discussion on the results and the main conclusions of this work are described, respectively.

2 Fundamentals

2.1 PET Systems

PET imaging uses radionuclides that decay by positron emission[10] and is performed after the administration of a radiotracer labelled with a positron-emitting radionuclide (β^+ particles). The method of acquisition is based on the coincidence detection of pairs of simultaneous anti-parallel photons that follow the annihilation of the positron emitted by the radionuclide with an electron of the tissue mean. This annihilation results in the production of two 511 keV gamma photons with an angle of approximately 180º apart from each other[7][10]. This way, a PET acquisition will eventually result in a number of these positron annihilation events detected by a ring of scintillation detectors.

Once one gamma photon is detected, the system will determine whether a second photon has been detected in a short time, which is referred to as *coincidence window*, which is typically 4-5 nanoseconds. If this occurs, the event is referred to as a *prompt coincidence*.

The virtual line defined between the points of detection of the two 511 keV gamma photons and is referred to as *line of response* (LOR), giving an estimative on the localization where the annihilation occurred[7][10]. Acquisition from detector pairs at various angular views, followed by an image reconstruction process, allows for an estimation of the biodistribution of the radiopharmaceutical within the image with a finite spatial resolution, sensitivity[7] and high efficiency[10].

Ideally, every prompt coincidence event should represent the LOR that passes through the annihilation point from which the two detected 511 keV gamma photons originated. However, to represent a prompt coincidence event, there are three types of events that can occur: *true coincidence* (A), *scattered coincidence* (B) and *random coincidence* (C), which are illustrated in Figure 2.1.

True coincidence occurs when two gamma photons originate from the same annihilation and do not change direction through scattering. In this case, the LOR intercepts the true origin of the annihilation. Scattered coincidences happen when one or both gamma photons originate from the same annihilation event undergo Compton scatter within the patient, changing the direction and ultimately creating an erroneous LOR. Finally, random coincidences occur when two single events from two unrelated annihilations are detected within a coincidence window originating a wrong LOR[19][20].

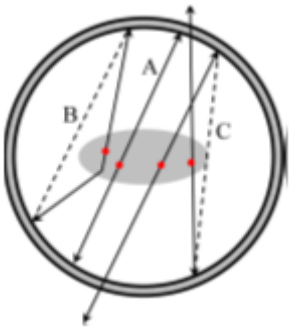

Figure 2.1 - Different types of coincidence events detected by a PET system: A) true coincidence events; B) scattered coincidence events, and; C) random coincidence events[19].

2.2 TOF Technology

In conventional PET, there is no information where, along the LOR, the annihilation occurred. However, in TOF-PET technology, the difference in the arrival times of two photons is measured with a finite precision in order to localize approximately the annihilation point along the LOR[19][20]. It exploits the time difference - Δt - in detection of the two photon events and correlates it to the position - Δx - of the annihilation point[7] in the LOR, to give a more precise estimation of localization of the annihilation in the *field of view* (FOV). The formula to calculate the position, is given as[7][14][21]:

$$\Delta x = \frac{c\Delta t}{2},$$

with *c* being the speed of light. This measured difference in detection time is directly related to the actual photon TOF difference, blurred by a measurement uncertainty named "*time resolution*"[6]. Hypothetically, with perfect TOF information, reconstruction would be unnecessary as the location of each annihilation could be identified as a fixed point in the LOR and therefore based only on the detected pair and time difference information[8]. In reality there is a finite timing resolution factors[6] and, therefore, TOF information is not adequate for the exact localization of the annihilation point along the LOR[6][7]. Nevertheless, imperfect timing information still helps to improve the reconstructed image because TOF information results in considerable gain in signal-to-noise ratio (SNR) by reducing the propagation of noise along the LOR[7][8][9]. A noise reduction can also be equated to an

increase in sensitivity[8], which also implies better lesion detectability and reduced radioactive dose received by the patient and/or reduced scan time[7].

2.3 Hybrid PET Systems

The basis of PET imaging is the detection of altered metabolism in biological tissues using radioactive tracers, enabling the assessment of cellular function. PET scans detect diseases at a metabolic level while anatomical imaging techniques such as CT or Magnetic Resonance Imaging (MRI) detect the disease at the morphological level.

PET uses rapid radioactive decay of positron emitting isotopes, such as fluorine-18 (F-18) and rubidium-82 (Rb-82), which, after their elution in cyclotron or in generator, are chemically introduced into molecules to assess biological functions. Since 2000, PET imaging has been migrating from the use of dedicated PET scanners to the standard use of PET-CT[15] or PET-MRI scanners.

In a hybrid PET-CT scanner, the PET and CT are housed in a single gantry. The CT is at the front of the gantry and the PET in at the back. State-of-art hybrid PET-CT scanners usually have a gantry size of 70 cm to allow the use of immobilization devices and accommodate larger patients[15]. The technologist uses the scout scan to define the starting and ending locations of the CT and PET acquisitions[25. The CT scan is acquired over the range previously defined and are usually obtained by using 100-140 kVp at various amperages, depending on the imaging protocol[15]. Upon the acquisition of the CT scan, the bed moves automatically to initiate the PET acquisition. One of the main advantages of a PET-CT scanner is the CT images used for attenuation correction of the PET data, providing better diagnostic accuracy and therefore, a more precise prognostic[1][15][16][21].

2.4 Attenuation Correction

Attenuation is the loss of gamma photons due to interactions with material and depends on the gamma photon energy and on the density of the attenuating material. The linear attenuation coefficient (μ) quantifies the relative reduction in detected counts and will differ throughout the body due to different tissue densities.

In PET, the attenuation is more pronounced because both photons are required to escape the material without interaction to create a true coincidence. As a gamma photon

passes through the material, the *total relative attenuation* (TRA) along the path length is calculated by:

$$\mathrm{TRA} = e^{-\mu x}$$

where μ corresponds to the linear attenuation coefficient an x corresponds to the path length.

For PET, it is a requirement to detect both 511 keV gamma photons that are emitted. In Figure 2.2, one may see that each gamma photon has its own TRA, according to the path length taken from point of emission. The joint probability of detecting both gamma photons is simply the multiple of the two TRA factors for each separate gamma photon.

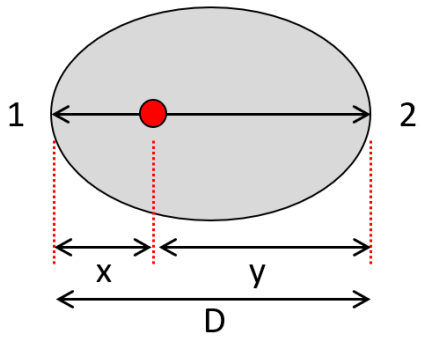

Figure 2.2 - Representation of the total relative attenuation (TRA) along the path length.

This gives a TRA for the line of response (TRA_{LOR}) of

$$\mathrm{TRA}_{LOR} = e^{-\mu x} \times e^{-\mu y} = e^{-\mu(x+y)} = e^{-\mu D}$$

This shows that the attenuation factor for the LOR is independent of the position of the annihilation along the LOR. When imaging over the thorax, there are different tissue densities, which makes it very non-uniform. This way a specific map of linear attenuation coefficient is required. The attenuation coefficient (AC) map is created by converting the voxel size of the CT slice to PET, then the Hounsfield Units are converted to linear attenuation coefficients (μ) using a lookup tale and then some smoothing is applied.

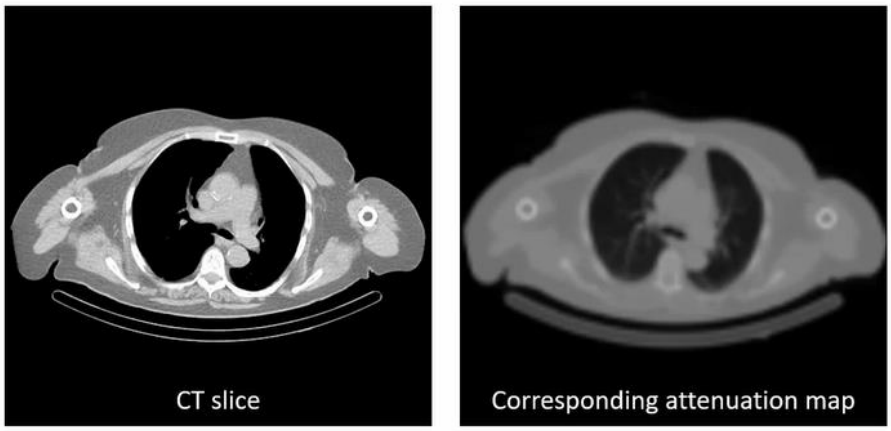

Figure 2.3 - The Hounsfield Units of the CT slice (left side) are converted into attenuation coefficients for a particular gamma photon energy, creating the attenuation map (right side).

Directly combining functional and anatomical information has been shown to improve the accuracy and efficiency of PET. However, the use of CT for attenuation correction of PET images has introduced artifacts that can affect the interpretation of the PET scan[1].

2.5 The truncation artifact

For the TRA of a given LOR to be correct, it must be possible to measure the distance between the two points on the patient's surface that the gamma photons exit from. During the creation of the attenuation map, this means that the entirety of the patient must be included in the transaxial field of view. If not, then the path length of the LOR will be underestimated and hence the attenuation will be underestimated.

In all available PET-CT systems today, standard transaxial FOV of CT is 50 cm, which is smaller than in the PET system, which is usually 70 cm. This difference in the maximum measured FOV between the two scanners may lead to truncation artifacts[15]. Consequently, the truncation artifact translates the discrepancy between the differences between the two FOVs, causing some sections of the PET emission data not to have any corresponding attenuation-correction map. Thus, it results in an underestimation corresponding to the region without attenuation-correction map[1].

This artifact can be induced if the patients are positioned incorrectly or have a larger abdominal perimeter. Although the mispositioning can be corrected and avoided by the technologist, the patient's size is not controllable.

Obesity is a growing medical condition in the modern society and therefore the diagnosis and assessment of various heart disease in obese patients are important for reducing

mortality and morbidity. Investigation on obese patients can be challenging because there is a higher risk of complications from invasive investigations and this way, it is very important to identify non-invasive techniques, such as PET-CT, that preserve the diagnostic and prognostic information in patients independently of the body mass index (BMI)[13]. Not surprisingly, the occurrence of truncation artifacts is more frequent in patients with large BMI.

Hybrid cardiac PET-CT with Rb-82 is a useful clinical tool for the diagnosis of unknown or suspected coronary arterial disease (CAD)[2] and microvascular disease, improving the understanding of the pathophysiology of disease processes thus directly impacting the therapeutic approach[12].

2.6 Cardiac PET-CT studies with Rb-82

Rb-82 is a potassium analogue and originates from the decay of strontium-82 (Sr-82) by electron capture. It is generator-produced, having a half-life of 75 seconds and decays into krypton-82 (Kr-82) by emitting a positron and a neutrino. It has a half-life that allows the generator to be eluted every 10 minutes, making Rb-82 suitable for sequential acquisitions[3].

The generator which produces the Rb-82 is stored in an automatic infusion system that guarantees accurate and reproducible elution. This infusion system is a mobile self-contained cart with a shield for the generator, a waste bottle shield, a saline syringe pump, sterile tubing and valve component, a detector and the console necessary for the administration to the patient – see Figure 2.4. This generator has a clinical life of 4 to 6 weeks[11][23].

Figure 2.4 - Rubidium infusion system present at the Nuclear Medicine Department of the Manchester Royal Infirmary.

There are daily mandatory quality control procedure requirements for radiochemical purity and eluate volume that must be performed on the generator and documented before using the radiopharmaceutical in the patient. This daily quality control consists of the generator column wash, a quality control testing requirement and the calibration test, and it takes, in total, approximately 75 minutes to complete.

Patients undergoing a Rb-82 myocardial perfusion study have the same preparation as any other myocardial perfusion imaging scan, which means they must be caffeine free for at least 12 hours prior the procedure and medications such as theophylline and aminophylline should be withheld 48 hours prior the scan day. In case of referrals for diagnosis of CAD cardiac medication and beta-blockers should be withheld for at least 48 hours prior exam[3].

When undergoing myocardial perfusion imaging with Rb-82, it is recommended to perform the rest images first to ensure there is enough time for a reduction of any residual stress effects such as ischaemic stunning and coronary steal[2] – see Figure 2.5.

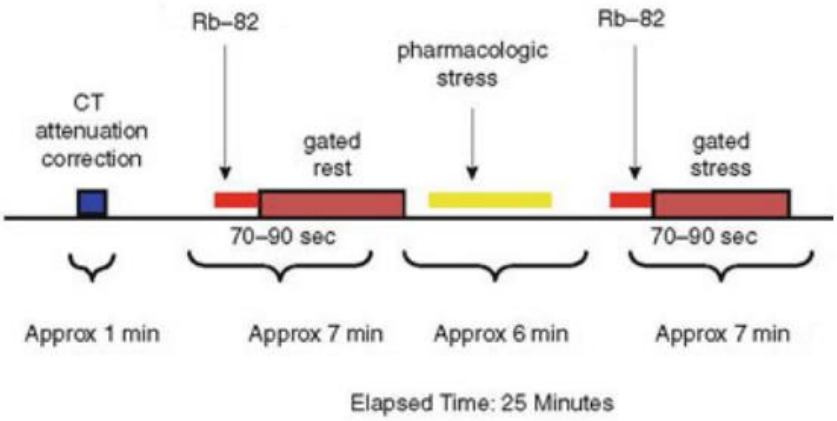

Figure 2.5 - Protocol of myocardial perfusion imaging with Rb-82[22].

After the injection of the tracer into the patient, the scan should be performed almost straight away. According to Dilsizian and colleagues[2], when the left ventricular ejection fraction (LVEF) is considered normal the acquisition should be performed within 70-90 seconds post injection. In cases of known decreased LVEF, it should start 90-110 seconds post injection. For LVEF below 30%, it is suggested to start the scan 110-130 seconds after[2]. This delay between the injection and the start of the acquisition of the study is required to increase the diagnostic accuracy of the study by ensuring adequate blood pool clearance. If the image was to be acquired sooner, counts that were not cleared from the residual blood pool would interfere with true counts originating from the myocardium.

Several images are generated from the PET acquisition of the Rb-82 data: these are static, ECG-gated and dynamic. The static images show the relative perfusion of Rb-82 at rest and stress and are assessed visually. The gated images show wall motion and help to identify wall motion abnormalities. Finally, the dynamic images capture the injection and the uptake into the myocardium and determine the absolute myocardial blood flow (MBF). The MBF can be used to detect balance three-vessel ischemia, which would be difficult to assess visually from the static images alone. For this project, only the static images are used as the impact of truncation on the relative static perfusion images is not known.

The Rb-82 myocardial perfusion imaging allows not only to improve image quality, spatial and diagnostic accuracy compared to SPECT-CT studies, but also a lower patient radiation exposure within a more rapid imaging procedure and a reliable prognosis and risk stratification. Nevertheless, this imaging study has some limitations such as the impossibility of performing exercise testing in patients due to the short half-life of the tracer.

The aim of this investigation is to evaluate the prevalence of the truncation artifact in the population undergoing a Rb-82 cardiac PET-CT study. Secondly, to evaluate the influence of TOF on the truncation artifact in cardiac PET-CT with Rb-82.

3 Methods

3.1 Objectives

This work aimed to answer 2 main questions:
1 – What is the prevalence of truncation artifacts in the CT images in the cardiac PET-CT exams acquired using Rb-82?
2 – Can the TOF technology help reducing the truncation artifact in these exams?

3.2 PET-CT Scanner

All patient scans were scanned on a Siemens Biograph Vision (Siemens Healthcare, Knoxville, TN) PET-CT system. This PET-CT has a bore diameter of 78 cm and a detector ring diameter of 82 cm. The detector is incorporated by lutetium orthosilicate scintillator (LSO) crystal and has 60,800 single element detectors, with 7,600 elements per ring. Each detector element has a size of 3.2×3.2×20 mm. The detectors elements are clustered in modules, with 200 per module. There is a total of 38 modules per ring with a total of 80 rings of detectors in the scanner. Each detector is also attached to a set of silicon photomultiplier (SiPM) detectors[17].

The axial FOV is defined by the number of rings, by the variation in the number of detectors per ring and by the distance between two parallel detectors. The transaxial FOV is 70 cm and the axial FOV is 26.3 cm[17]. The TOF timing resolution for the system is quoted as 214 ps.

All studies collected for this study included a CT scan. The incorporated CT in the Siemens Biograph Vision PET-CT has a standard of 64 acquired sliced and 192 reconstruction slices per rotation and a rotation time of 0.33 s. It has a scan field of 50 cm and an extended PET axial FOV of 21 cm, giving it a final 78 cm CT extended FOV.

The PET and the CT technical parameters used in the Nuclear Medicine Department of the Manchester Royal Infirmary for myocardial perfusion exams with Rb-82 are described as following in Table 3.1 and 3.2.

Table 3.1 - Technical Parameters of PET for Myocardial Perfusion with Rb-82.

Parameter	Value
Patient position	Head-first; Supine
Scan type	List mode
Time per bed	5 minutes
Reconstruction Static	Rest Static UHD or Stress Static UHD
Reconstruction Static parameters	Static Replay 150 to 300 seconds 128×128, zoom 2.5 (voxel size 2.0 mm × 2.0 mm) Match to CT spacing (132 slices) Pan (x, y) = (50, -20) UHD 4 iterations, 5 subsets, 6.0 mm filter
Reconstruction Gated	Rest Gated UHD or Stress Gated UHD
Reconstruction Gated parameters	Gated 8-frames Replay 150 to 300 seconds 220×220, zoom 2.0 (voxel size 2.0 mm × 2.0 mm) Match to CT spacing (1056 slices) UHD 4 iterations, 5 subsets, 6.0 mm filter
Reconstruction Dynamic	Gated 8-frames Replay 150 to 300 seconds 220×220, zoom 2.0 (voxel size 2.0 mm × 2.0 mm) Match to CT spacing (1056 slices) UHD 4 iterations, 5 subsets, 6.0 mm filter
Reconstruction Dynamic parameters	Rest Dynamic TOF or Stress Dynamic TOF Dynamic 21 frames 10×5 seconds, 4×10 seconds, 7×30 seconds 128×128, zoom 2.5 (voxel size 2.0 mm × 2.0 mm) Match to CT spacing (2772 slices) Pan (x, y) = (50, -20) UHD 4 iterations, 5 subsets, 6.0 mm filter

Table 3.2 - Technical Parameters of CT for Myocardial Perfusion with Rb-82.

Parameter	Value
Tube voltage	120kVp
Tube current	11 mAs (quality reference) for patient below 115 kg 20 mAs (quality reference) for patient above 115 kg
Beam collimation	16×1.2 mm
Helical Pitch	1.5
Rotation time	0.5 s
Kernel	B19f for attenuation correction
FOV	700 mm
Helical pitch	1.5
Slice thickness	3.0 mm
Slice spacing	2.0 mm

3.3 Selection of sample

150 consecutive resting scan images were included in this study. The aim was to assess any artefact caused in a normally perfused myocardium. For this reason, only the rest images were included in this project. 73 resting studies were selected by the author of this work based on good quality images with no extra cardiac activity near the heart. Images with excessive extra cardiac activity were excluded as this may interfere with the analysis.

The sample was collected between October 2019 and February 2020.

3.4 Patient preparation prior to the image acquisition

Every patient undergoing a myocardial perfusion exam with Rb-82 at the Nuclear Medicine Department of the Manchester Royal Infirmary must have a relevant clinical indication and a referral previously justified by the doctor on site. It is the hospital policy (guided by IRMER[30]) and it is mandatory to verify the identity of every patient undergoing any scan. If relevant, information such as pregnancy and/or breast-feeding status should be written down as well.

The protocol adopted by the department is a single session rest/stress protocol and therefore, both rest and stress procedures are done in the same day. The preparation for the pharmacology stress procedure includes various checks and therefore, it is important to go over each and all of them to assure everything is being done within the national and the department guidelines, as follow:

- Ensure patient has been caffeine free for 12 hours.
- Asthma (to see which stress pharmaceutical is suitable).
- Diabetes, more in particular if the patient has missed any medication or meal or if it is insulin dependent as it increases the risk of hypoglycaemia. When on doubt, we need to measure the blood glucose.
- Ensure the patient is not currently taking any contraindicated medication as some medication need to be stopped prior the stress procedure, such as the one listed in Table 3.3;
- Evaluate if the patient will be able to comply with the desirable position for the scan – both arms above their heads. If the patient is unable to lie with both arms up, assess if they can manage with the left arm up and use that arm for the rubidium cannula. It is possible to scan with both arms alongside their bodies, however if the patient is large this may compromise the image quality.

Table 3.3 - List of medications contraindicated for the use of Adenosine.

Medication contraindicated with Adenosine
Persantin (Dipyridamole)
Methyl Xanthines
Aminophylin (Phyllocotin)
Theophylline (Uniphyllin)

As this scan is performed in cardiac-gated mode, it is necessary to position the 10 electrodes for the 12-lead echocardiogram (ECG). Three (3) extra electrodes need to be placed for the Myocardial Perfusion Gating – both wrists and left hip. Before starting the Rest/Stress procedure, one needs to ensure that the patient has understood the overall procedure of the exam and that he/she is able to give a verbal consent before insert an intravenous (IV) cannula.

Every patient laid down on the bed, prior to the explanation of the procedure, in supine and head-first position. An adequate arm support was used every time and if needed; a knee

support pillow was offered for a better comfort. We also measured the patient's blood pressure due to the nature of the procedure. If possible, measure the pressure using the opposite arm of the cannula, however, if there is a cannula in both antecubital fossa regions, and then take the measures from the arm where the IV Rb-82 cannula was inserted. The 12-lead ECG will posteriorly be connected to the *Cardiosoft* ECG box – system used in the department.

While positioning the patient, we always made sure the cannula was accessible for use during the procedure – Rb-82 rest injection, followed by the pharmacology stress and Rb-82 stress injection.

When working with any radioactive substance and source, one should always take care to minimize the radiation exposure to everyone involved – patient and personnel – relying on consistent applicability[20] of all physical and radiation protection principles, including the optimization and the ALARA (*As Low As Reasonably Achievable*) ones.

All exams were collected without exposing the patient and the personnel to a radiation dose other than the strictly necessary to accomplish the defined protocol.

3.5 Rb-82 Infusing System Generator: CardioGen-82

The CardioGen-82 Infusion system is an automatic system[20] used for the generation of Rb-82 from Sr-82 and delivery of Rb-82 to a patient to evaluate cardiovascular conditions.

For every patient undergoing a myocardial perfusion exam with Rb-82, a standard dose of 20 mCi (740MBq) is given and the flow rate of infusion – in accordance with the CardioGen-82 package insert – is of 50 mL/min for each elution – both for Rest and Stress studies. Furthermore, it was also selected 20 mL as the volume administrated to the patient and 40 mL as the total volume pumped through the generator during an infusion. These two volumes are standard for any patient with a body mass bellow 115 Kg. Finally, the dose rate threshold is 1.0 mCi/sec, to help controlling when the system will directly eluate to the patient. The infusion continues and stops when it reaches the patient dose – which is the normal stopping limit.

3.6 Image Acquisition Protocol

Before starting the acquisition, the protocol was selected depending on the weight of the patient to best suit the body mass (standard protocol and above 150 kg protocol). The quality *ref mAs* parameter is also adapted depending on the weight – if the patient is above 115 kgs, we changed from 11 to 20 *mAs*. Figure 3.1 shows the electronic setting and how to change the quality *ref mAs*. The CT voltage is settled at 120 kVp, with a helical pitch of 1.5, beam collimation of 16×1.2 mm and a rotation of 0.5 s.

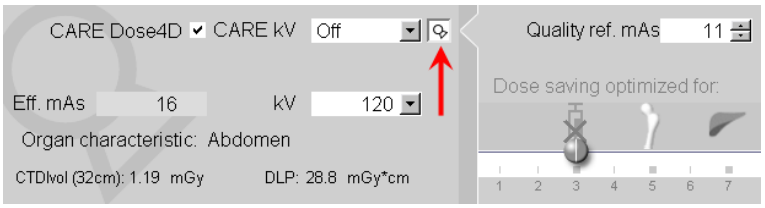

Figure 3.1 - Quality ref mAs setting GUI in Syngo workstation – Siemens.

A scout image was acquired before starting the actual scan to delimitate the CT FOV. An area between the bifurcation of trachea – carina – and the end of the ribcage was selected for the FOV, taking into consideration that the heart is centralized in it. Figure 3.2 is an illustration of the adjusting of the FOV.

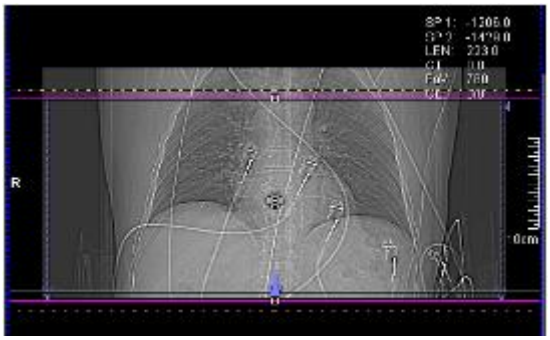

Figure 3.2 - Scout image for PET Myocardial acquisition using Rb-82.

The CT acquisition is performed, followed by the PET acquisition. Before the start of the PET acquisition, the technician enters the room to start the Rb-82 infusion for the Rest. The infusion only starts when the rubidium cart changes its light to waste from patient. The scan is therefore started when the count-rate starts to increase on the graphic in the acquisition

panel, as showed in figure 3.3. This slight delay between the injection of the tracer and the beginning of the PET acquisition is needed to increase the diagnostic accuracy of the scan.

Figure 3.3 - PET Acquisition Monitor panel in the form of a graph for the detection of True and Random events.

After starting the scan, a note on the scanning sheet was written if the patient moved during the acquisition. The Rest procedure lasts for 5 minutes.

During the processing of the rest images, the stress team is already preparing the patient for the stress procedure. Depending on the pharmacological drug, the second infusion of Rb-82 should be injected into the patient in a 10-minute window since the beginning of the rest injection. At 4 minutes, after the start of the acquisition, the images of the acquisition will be displayed, and the registration of the PET and CT should be checked. After the completion of this second part, the reconstruction of the images should be performed.

3.7 CT Image Reconstruction and Truncation Evaluation

CT reconstructions were performed with the standard 50 cm FOV and the 78 cm extended FOV. The extended CT images also included a red overlay indicating the extent of the standard 50 cm FOV – see Figure 3.4. This allowed for identification of truncation on the 50 cm FOV images when any part of the patient was positioned outside the extent of the red line. Figure 3.4 shows an example without truncation and two examples with truncation on the 50 cm FOV. The red dashed line shows the 50 cm FOV. The occurrence of truncation artifact on patient images, in the 50 cm FOV, was identified by the author of this study and one of the supervisors, on a pure visual basis, and performed by applying a wide image

window to the CT, which showed the extent of the reconstructed FOV. This can be visualised by the dark grey circle on the images in Figure 3.4. If any part of the patient was seen to me missing outside this reconstructed FOV then truncation in the extended FOV was assumed.

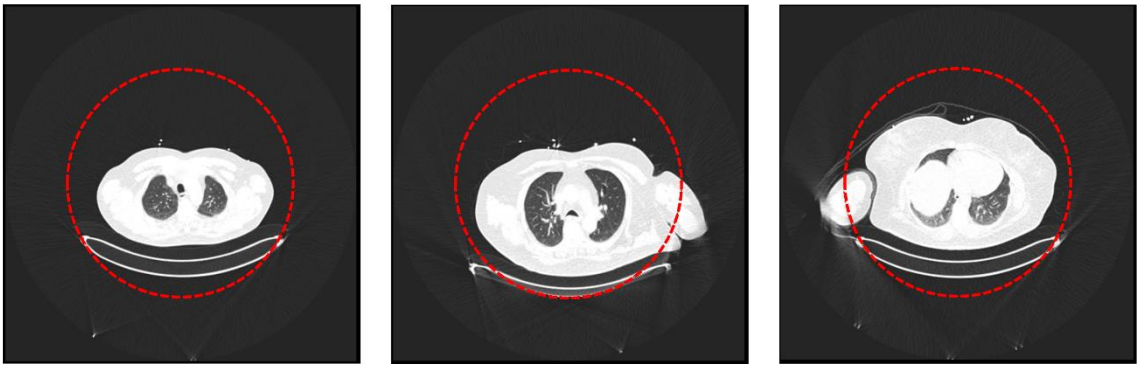

Figure 3.4 - Example CT images showing cases without truncation (left) (Male BMI 28.3 kg/m^2, arms up) and two examples with truncation (center: Female BMI of 39.1 kg/m^2 and left arm down; right: Female BMI of 33.7 kg/m^2 and right arm down)

Following the visual analysis and separation in these two different categories**,** the static PET images were reconstructed with and without TOF. The details taking into consideration for both reconstructions is listed in the following Table 3.4.

Table 3.4 - Details of TOF and Non-TOF Reconstructions.

	TOF Reconstruction	Non-TOF Reconstruction
Reconstruction method	True X + TOF (HD-PET)	True X (HD-PET)
Iterations	4	12
Subsets	5	5
Image Size	440	440
Zoom	1.0	1.0
Filter	Gaussian	Gaussian

TOF and Non-TOF PET images were reconstructed with both the 50cm CT and extended FOV CT. A ratio image was produced by dividing the voxel values of the PET using the 50cm CT by the voxel values of the PET using the extended CT image on a voxel by-voxel basis. A mask region was generated by a threshold of the mean image to a percentage of the maximum voxel value within the cardiac insert. The threshold was set manually following visual inspection of the mask. This mask was then transposed onto the ratio image and the

mean value of voxels within the mask on the ratio image was calculated. The analysis was performed only on the image volume that contained the cardiac insert. This was to avoid the inclusion of high uptakes of extra-cardiac activity that are common to be observed in the clinical image. Any extra-cardiac activity that would not allow to produce an effective mask on the image would lead to the exclusion of the selected image. Figure 3.5 shows a schematic of how the mask was produced.

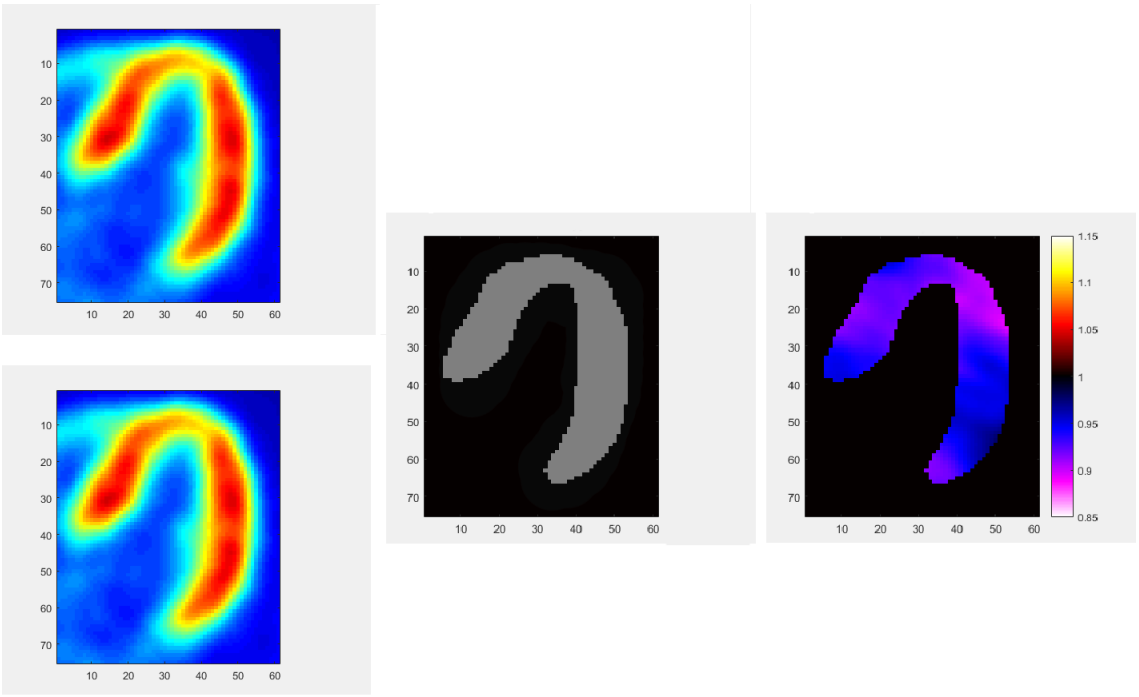

Figure 3.5 - Schematic to show the creation of a masked ratio image.

The two images reconstructed with 50 cm and EFOV CT are shown on the left in the Figure 3.5. The centre image shows the mask image derived from the left ventricle intensity and the right image show the ratio image (50 cm CT/EFOV CT) with the mask applied.

The voxel values from within the masked ratio image were extracted and the mean and standard deviation of these values were calculated. These calculations would show different things from the ratio images. A mean greater than or less than 1 combined with a low standard deviation would indicate a systematic offset in all voxel values. This situation would not produce images with significant visual differences. Cases where the standard deviation was high, irrespective of the mean, would indicate regional differences in the myocardial uptake in the two PET images reconstructed with the different CT images. This situation may be expected to produce images with notable visual differences.

3.8 Visual Analysis of the Images

To analyse the images, the PET static images were separated into two groups: images with truncation artifact and images without the artifact. Within each group, the images were paired into TOF and Non-TOF reconstructed and were visually evaluated. A score system from 0 to 2 was created, being 0 classified as no difference perceivable, 1 as subtle perceivable difference and 2 classified as clear perceivable difference.

3.9 Statistical Analysis

All statistical analysis was performed using Statistic software SPSS version 23.0 for Windows. The data collected regarding the presence of the truncation artifact was of 27 resting studies and therefore, based in the statistical tests used, the comparison between this variable with other or others, *n* was automatically assumed as 27 and not 26 (*n*-1) due to the lack of information.

The results were considered significant at 5% of significance level. To test the normality of the data obtained through the calculation of ratio image, the Shapiro-Wilk test was used. Afterward, the Wilcoxon rank test was used to test for paired reconstructions, in other words, to compare the voxel ratio mean in areas where the truncation artifact was present with and without TOF and the voxel ratio mean in images where the truncation artifact was not present with and without TOF.

To compare unpaired groups, relatively to the presence (or not) of truncation artifact, it was used the Mann-Whitney U-test since the assumption of normality was not verified.

4 Results

4.1 Sample results

In the 73 collected studies, 46 resting studies did not show truncation of the 50 cm CT images. The remaining 27 resting studies showed evidence of truncation of the 50 cm CT images. However, no cases showed truncation of the eFOV CT images.

	No truncation	Truncation of 50 cm FOV
Sex	24 M	16 M
	22 F	11 F
BMI (median)	28.9	36.1

Out of these 27 showing truncation, studies, 18 studies were acquired with both arms up, 8 studies with the left arm down and 1 study with the right arm down. It was verified that out of the 27 patients that yielded truncation artifacts, 22 had a BMI classified as obese. From this simple analysis, it was concluded that the habitus of the patient and the position of the arms contributed to the presence of the truncation artifact. Bad positioning on the bed was also assessed as an important cause of the truncation artifact, which is in accordance to several authors[26] [27] [28

4.2 Normality and paired tests

A Shapiro-Wilk test was performed to test the normality of the data obtained through the calculation of ratio image, yielding a *p* value lower than 0.05.

Figures 4.1 and 4.2 show the analysis of the voxel values within the masked ratio images where the ratios are voxels in the PET images using the 50 cm and EFOV CT for attenuation correction as illustrated in Figure 3.4.

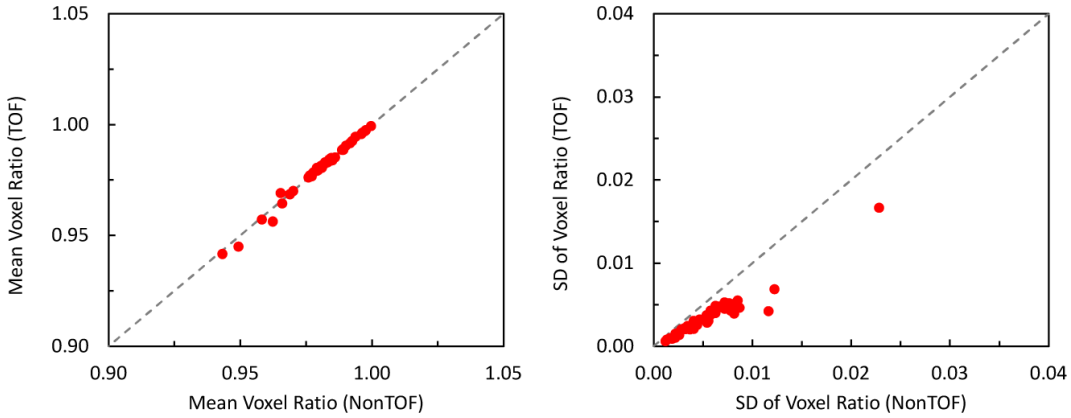

Figure 4.1 - Mean value and standard deviation of the voxel values within the masked ratio images for non-truncated cases.

In the Figure 4.1 on the left side shows the comparison of the mean value of the voxel ratios (50cm/EFOV) within with mask applied to the ratio images. On the right, the standard deviation of the voxel ratios. These plots are for the cases that showed no evidence of truncation of the 50 cm CT images.

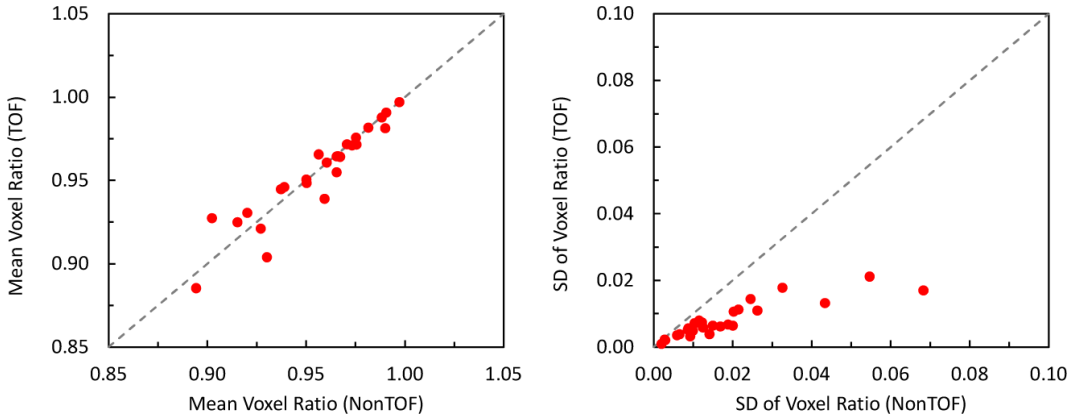

Figure 4.2 - Mean value and standard deviation of the voxel values within the masked ratio images for truncated cases.

On the left side in the Figure 4.2 shows a comparison of the mean value of the voxel ratios (50cm/EFOV) within with mask applied to the ratio images. On the right boxplot the standard deviation of the voxel ratios. These plots are for the cases that showed evidence truncation of the 50 cm CT images.

The boxplots in Figures 4.3 and Figure 4.4 show the distribution of the ratio mean and ratio standard deviation, respectively, in the masked images. Distributions are shown for TOF and non-TOF reconstructions for truncated and non-truncated cases.

A significant difference in the standard deviation can be observed when compared between truncated and non-truncated cases.

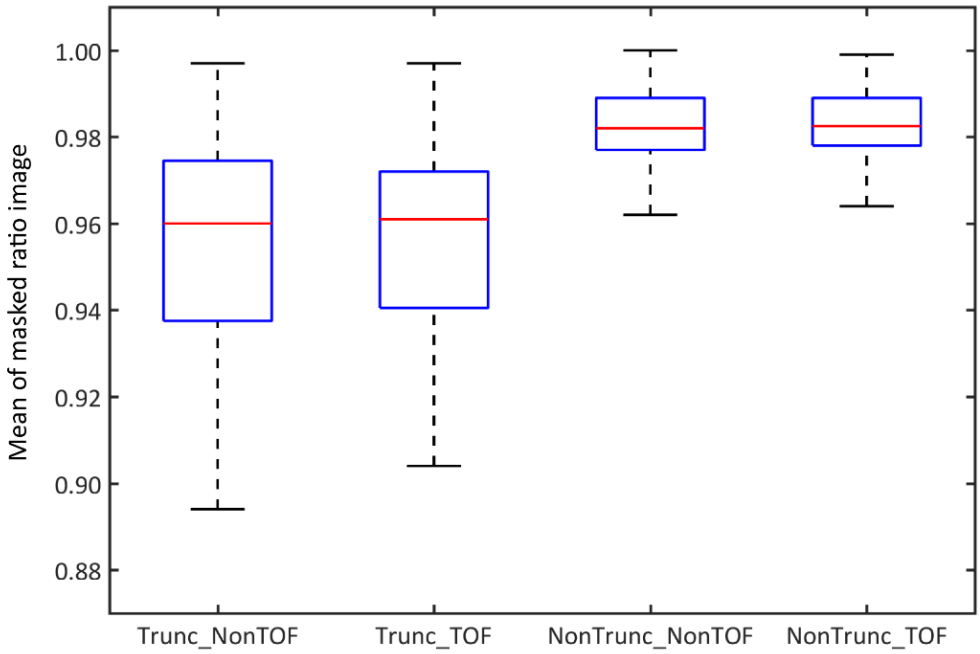

Figure 4.3 - Boxplot of the mean of the masked ratio image between truncated and non-truncated groups.

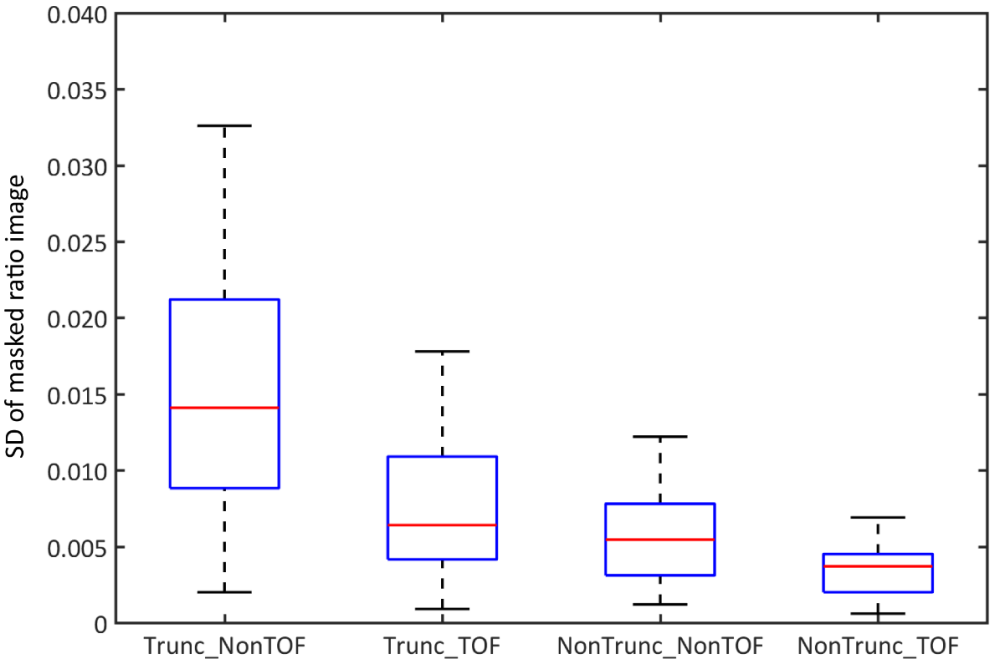

Figure 4.4 - Boxplot of the standard deviation of the masked ration image between truncated and non-truncated groups.

A Wilcoxon rank test was then calculated, and its results can be observed in Tables 4.1 and 4.2. This test is a nonparametric one used for paired data based on independent units of analysis and, for this project, it was performed to evaluate the non-TOF reconstructions versus the TOF reconstructions for the group where truncation was present and the non-TOF reconstructions versus TOF reconstructions for the group where truncation was not present.

In Table 4.1, it is observed that the *p* value is significantly greater than 5% and in the Table 4.2 the *p* value is significantly greater than 0.05.

Table 4.1 - Wilcoxon rank test for paired reconstructions of the truncated voxel ratio mask mean (non-TOF vs TOF).

Hypothesis Test Summary

	Null Hypothesis	Test	Sig.	Decision
1	The median of differences between Mean (ratio) non TOF and Mean (ratio) TOF equals 0.	Related-Samples Wilcoxon Signed Rank Test	,665	Retain the null hypothesis.

Asymptotic significances are displayed. The significance level is ,05.

Table 4.2 - Wilcoxon rank test for paired reconstructions of the non-truncated voxel ratio mask. mean (non-TOF vs TOF).

Hypothesis Test Summary

	Null Hypothesis	Test	Sig.	Decision
1	The median of differences between Mean nonTOF (ratio) and Mean TOF (ratio) equals 0.	Related-Samples Wilcoxon Signed Rank Test	,939	Retain the null hypothesis.

Asymptotic significances are displayed. The significance level is ,05.

In Figure 4.3, it is exemplified the difference between the ratio image in the truncated and non-truncated in TOF and non-TOF reconstructions. This corroborates the Wilcoxon test results. Besides, it is observed a visual difference between the truncated versus the non-

truncated group, whose statistical significance was also assessed. This was done using a nonparametric approach – the Mann-Whitney U-test – since the data are not normally distributed. The test was applied to assess the difference between the truncated and the non-truncated group.

In Table 4.3, the TOF voxel ratio mean from truncated versus non-truncated has also a *p* value < 0.05.

Table 4.3 - Mann-Whitney U-test for TOF voxel ratio mask mean (truncated vs. non-truncated).

Ranks

		N	Mean Rank	Sum of Ranks
Mean nonTOF (ratio)	Truncated	27	22,59	610,00
	Non-Truncated	46	45,46	2091,00
	Total	73		

Test Statistics[a]

	Mean nonTOF (ratio)
Mann-Whitney U	232,000
Wilcoxon W	610,000
Z	-4,445
Asymp. Sig. (2-tailed)	,000

a. Grouping Variable: Truncated vs non-truncated

When comparing the voxel value between non-TOF and TOF, it can be observed a significantly greater variation in the truncated images compared with the non-truncated images.

4.3 Visual Quality Assessment

Table 4.4 describes the visual analysis of 146 reconstructions and classifies them into 3 score groups depending on the perceptive visual difference between truncated and non-truncated images, with and without TOF. The visual quality assessment was performed by a physic from the department, who classified the images into the 3 score groups without previously knowing if they were truncated or not.

Out of the 46 which were classified as having the truncation artifact, 1 TOF truncated image and 2 non-TOF truncated images were classified with a score of 1 and 2 non-TOF truncated images were classified with a score of 2 from the visual quality assessment. The rest of the truncated images were classified with a score of 0. Within the group of non-truncated, only 1 non-TOF image was classified with a score of 1.

Table 4.4 - Score of the visual differences on the reconstructions.

		Score		
		0	**1**	**2**
Truncated	**TOF**	26	1	0
	Non-TOF	23	2	2
Non-truncated	**TOF**	46	0	0
	Non-TOF	45	1	0

From the visual analysis, it is concluded that there is no significant difference when comparing between non-TOF against TOF within the truncated images compared with the non-truncated images.

5 Discussion

The difference between the PET and the CT scanners may lead to truncation artifacts, causing some sections of the PET emission data not to have any corresponding attenuation-correction map. This project has evaluated the prevalence and impact of truncation of CT images, used for attenuation correction in rubidium myocardial perfusion PET. There appears to be very few studies that have studied the impact of truncation specifically in cardiac PET imaging. Mawlawi et al investigated truncation in phantoms and a small group of five FDG oncology whole-body scans. From their investigation, by using a method described by Hsieh et al that extends the projections that are truncated expecting that the total attenuation of each projection remains constant over all views, they concluded that a correction algorithm can be applied to correct this artifact in different types of body densities with a small error.

Also, Beyer et al studied truncation, in phantom images and in a small group of 10 FDG oncology scans. From their study, it was also concluded that by applying using an extended CT FOV helps to recover activity in the PET emission data.

In additional there appears to be very little work studying the benefits of TOF in the presence of truncated CT. In a conference presentation, Ochoa et al compared TOF and non-TOF reconstructions of images. The authors added additional saline bags to the phantom, increasing its size to the point that it because truncated on the CT.

The main focus of addressing truncation in PET images has been directed towards PET-MR[31][32] [33].

5.1 Prevalence of truncation

This work has shown that truncation of the standard FOV of the CT occurs in 37% of patients (27/73). In all available PET-CT systems today, standard transaxial FOV of CT is 50 cm, which is smaller than in the PET system, which is usually 70 cm. This difference in the maximum measured FOV between the two scanners may lead to truncation artifacts. Consequently, the truncation artifact translates the discrepancy between the differences between the two FOVs, causing some sections of the PET emission data not to have any corresponding attenuation-correction map. Thus, it results in an underestimation corresponding to the region without attenuation-correction map.

The habitus of the patient and the position of the arms contributed to the presence of this artifact. Also the bad position on the bed was also assessed as an important cause of the truncation artifact, which is in accordance to several authors.[26] [27] [28

5.2 Impact of truncation

This primary metric used to quantify differences in the PET images reconstructed in situations with truncated CT was the ratio of the PET voxels. The standard deviation of these voxel ratio within the left ventricle was calculated and illustrated the magnitude of spatial variation of the differences in the with and without truncation. This was performed for TOF and non-TOF reconstructions to show benefits of using TOF reconstruction.

When comparing the standard deviation of the voxel ratios for non-TOF and TOF reconstructions, it was shown that non-TOF resulted in a significantly greater variation of ratios. This illustrates that the use of TOF reconstruction can significantly reduce the impact of quantitative changes in PET reconstructions compared with non-TOF reconstruction, which can be confirmed with the literature.[24]

It was verified that when compared between male and female there was no significant differences on the impact of the truncation artifact.

5.3 Limitations

This project did not perform phantom study due to the lack of suitable available phantoms to indicate truncation. Phantom studies would allow to do a ground truth. Also, the fact that the sample was small (<100) did not allow to have a better notion of the impact of the artifact. A larger patient study group would allow better separation into various BMI groups to study the truncation more thoroughly. No attempt was made to quantify the degree of truncation on the CT images as this was challenging due to the lack of precise CT data in truncated images.

6 Conclusion

The combined high-resolution morphological CT images with the functional image of PET became a significant advantage for clinical imaging utility, providing a better diagnostic accuracy and consequently, a more precise prognostic. Nevertheless, the use of CT for attenuation correction of PET images can introduce artifacts which can affect the interpretation of the PET scan.

From the aim of this investigation, which was to evaluate the prevalence of the truncation artifact in the population and to evaluate the influence of TOF on the truncation artifact in cardiac PET-CT with Rb-82, it is concluded that the use of TOF information in reconstruction enables to reduce the impact of the CT truncation and therefore is the method of choice for patients with large body mass index.

Bibliography

[1] Mawlawi O, Erasmus JJ, Pan T, Cody DD, Campbell R, Lonn AH, et al. Truncation Artifact on PET/CT: Impact on Measurements of Activity Concentration and Assessment of a Correction Algorithm. American Journal of Roentgenology. 2006;(186):1458–67.

[2] Dilsizian V, Bacharach SL, Beanlands RS, Bergmann SR, Delbeke D, Gropler RJ, et al. PET myocardial perfusion and metabolism clinical imaging. J Nucl Cardiol. 2009 Aug 1;16(4):651–651.

[3] Yoshinaga K, Klein R, Tamaki N. Generator-produced rubidium-82 positron emission tomography myocardial perfusion imaging - From basic aspects to clinical applications. Journal of Cardiology. 2010;(55):163–73.

[4] Tong S, Alessio AM, Thielemans K, Stearns C, Ross S, Kinahan PE. Properties and Mitigation of Edge Artifacts in PSF-Based PET Reconstruction. IEEE Transactions on Nuclear Science. 2011 Oct;58(5):2264–75.

[5] Harnett DT, Hazra S, Maze R, Mc Ardle BA, Alenazy A, Simard T, et al. Clinical performance of Rb-82 myocardial perfusion PET and Tc-99m-based SPECT in patients with extreme obesity. J Nucl Cardiol. 2019 Feb 1;26(1):275–83.

[6] Conti M. State of the art and challenges of time-of-flight PET. Physica Medica. 2009 Mar 1;25(1):1–11.

[7] Spanoudaki VCh, Levin⋆ CS. Photodetectors for Time-of-Flight Positron Emission Tomography (ToF-PET). Sensors (Basel). 2010 Nov 18;10(11):10484–505.

[8] Karp JS, Surti S, Daube-Witherspoon ME, Muehllehner G. The benefit of time-of-flight in PET imaging: Experimental and clinical results. J Nucl Med. 2008 Mar;49(3):462–70.

[9] Lois C, Jakoby BW, Long MJ, Hubner KF, Barker DW, Townsend DW, et al. An Assessment of the Impact of Incorporating Time-of-Flight (TOF) Information into Clinical PET/CT Imaging. J Nucl Med. 2010 Feb;51(2):237.

[10] Machac J. Cardiac positron emission tomography imaging. Semin Nucl Med. 2005 Jan;35(1):17–36.

[11] Arumugam P, Tout D, Tonge C. Myocardial perfusion scintigraphy using rubidium-82 positron emission tomography. Br Med Bull. 2013; 107:87–100.

[12] Chilra P, Gnesin S, Allenbach G, Monteiro M, Prior JO, Vieira L, et al. Cardiac PET/CT with Rb-82: optimization of image acquisition and reconstruction parameters. EJNMMI Phys. 2017 Feb 15;4(1):10.

[13] Chow BJW, Dorbala S, Di Carli MF, Merhige ME, Williams BA, Veledar E, et al. Prognostic Value of PET Myocardial Perfusion Imaging in Obese Patients. JACC: Cardiovascular Imaging. 2014 Mar 1;7(3):278–87.

[14] Budinger TF. Time-of-flight positron emission tomography: status relative to conventional PET. J Nucl Med. 1983 Jan;24(1):73–8.

[15] Anand S, Singh H, Dash A. Clinical Applications of PET and PET-CT. Med J Armed Forces India. 2009 Oct;65(4):353–8.

[16] Beyer T, Bockisch A, Kühl H, Martinez M-J. Whole-body 18F-FDG PET/CT in the presence of truncation artifacts. J Nucl Med. 2006 Jan;47(1):91–9.

[17] Tong S, Alessio AM, Kinahan PE. Image reconstruction for PET/CT scanners: past achievements and future challenges. Imaging Med. 2010 Oct 1;2(5):529–45.

[18] Snyder DL, Miller MI, Thomas LJ, Politte DG. Noise and edge artifacts in maximum-likelihood reconstructions for emission tomography. IEEE Trans Med Imaging. 1987;6(3):228–38.

[19] Armstrong I. Quantitative accuracy of iterative reconstruction algorithms in positron emission tomography [Ph.D.]. University of Manchester; 2017

[20] Surti S. Update on time-of-flight PET imaging. J Nucl Med. 2015 Jan;56(1):98–105.

[21] Townsend DW, Beyer T. A combined PET/CT scanner: the path to true image fusion. Br J Radiol. 2002 Nov;75 Spec No: S24-30.

[22] CardioGen-82® (Rubidium Rb 82 Generator) | Bracco Imaging

[23] Armstrong IS, Tonge CM, Arumugam P. Assessing time-of-flight signal-to-noise ratio gains within the myocardium and subsequent reductions in administered activity in cardiac PET studies. J Nucl Cardiol. 2019 Apr 1;26(2):405–12.

[24] Ochoa MG, Wells K, Mahmood S. Time-of-flight (TOF) PET versus non-TOF PET reconstructions with truncated CT attenuation map. J Nucl Med. 2012 Jan 5;53(supplement 1):2348–2348.

[25] Sureshbabu W, Mawlawi O. PET/CT Imaging Artifacts. J Nucl Med Technol. 2005 Jan 9;33(3):156–61

[26] Uppot RN, Sahani DV, Hahn PF, Gervais D, Mueller PR. Impact of Obesity on Medical Imaging and Image-Guided Intervention. American Journal of Roentgenology. 2007 Feb 1;188(2):433–40.

[27] Reynolds A. Obesity and Medical Imaging Challenges. Radiol Technol. 2011 Jan 1;82(3):219–39.

[28] Uppot R. Technical challenges of imaging & image-guided interventions in obese patients. The British Journal of Radiology. 2018 Jun 5; 91:20170931.

[29] Jiang Hsieh, Computed Tomography: Principles, Design, Artifacts, and Recent Advances, Second Edition, 2009.

[30] Ionising Radiation (Medical Exposure) Regulations 2017: guidance. GOV.UK

[31] Blumhagen JO, Braun H, Ladebeck R, Fenchel M, Faul D, Scheffler K, et al. Field of view extension and truncation correction for MR-based human attenuation correction in simultaneous MR/PET imaging. Medical Physics. 2014;41(2):022303.

[32] Oehmigen M, Lindemann ME, Gratz M, Kirchner J, Ruhlmann V, Umutlu L, et al. Impact of improved attenuation correction featuring a bone atlas and truncation correction on PET quantification in whole-body PET/MR. Eur J Nucl Med Mol Imaging. 2018 Apr 1;45(4):642–53.

[33] Tang J, Haagen R, Blaffert T, Renisch S, Blaeser A, Salomon A, et al. Effect of MR truncation compensation on quantitative PET image reconstruction for whole-body PET/MR. In: 2011 IEEE Nuclear Science Symposium Conference Record. 2011. p. 2506–9.